Journal of the European Ceramic Society 22 (2002) 2333–2342
www.elsevier.com/locate/jeurceramsoc

Mullite (Nextel^{TM} 720) fibre-reinforced mullite matrix composites exhibiting favourable thermomechanical properties

C. Kaya[a,*], E.G. Butler[a], A. Selcuk[b], A.R. Boccaccini[b], M.H. Lewis[c]

[a]*Interdisciplinary Research Centre (IRC) in Materials Processing, The University of Birmingham, Edgbaston, Birmingham, B15 2TT, UK*
[b]*Department of Materials, Imperial College of Science, Technology and Medicine, Prince Consort Road, London, SW7 2BP, UK*
[c]*Department of Physics, Centre for Advanced Materials, University of Warwick, Coventry, CV4 7AL, UK*

Received 25 September 2001; accepted 8 December 2001

Abstract

A mullite matrix containing homogeneously distributed ultra-fine (70–350 nm) pores was reinforced with $NdPO_4$-coated woven mullite fibre mats (Nextel^{TM} 720) leading to damage-tolerant composites with good high temperature (1300 °C) strength and thermal cycling resistance. Electrophoretically deposited fibre preforms were placed in a high-load pressure filtration assembly, leading to formation of consolidated compacts with high green densities. After sintering at 1200 °C for 3 h, the compacts had a density of 86.4% of theoretical density and showed damage-tolerant behaviour up to 1300 °C, with flexural strength values of 235 MPa and 224 MPa at room temperature and 1300 °C, respectively. No significant microstructural damage was detected after thermal cycling the samples between room temperature and 1150 °C for up to 300 cycles. The thermomechanical test results combined with detailed electron microscopy observations indicate that the overall composite behaviour in terms of damage-tolerance, thermal capability and thermal cycling resistance is mainly controlled by two microstructural features: (1) the presence of a dense $NdPO_4$ interphase but weak bonding with the matrix or fibre and (2) the presence of homogeneously distributed nano pores (<350 nm) within the mullite matrix.

Keywords: Composites; Fibres; Mechanical properties; Microstructure-final; Mullite; Mullite fibres; Thermal cycling

1. Introduction

Continuous fibre-reinforced ceramic matrix composites have attracted significant scientific and technological interest for high temperature structural applications due to their damage-tolerant behaviour, decreased flaw sensitivity and resistance to creep.[1–4] The development of oxide fibre-reinforced oxide matrix composites is a promising means of achieving lightweight, structural materials combining high-temperature strength with improved fracture toughness, damage tolerance, thermal shock and oxidation resistance. Significant research effort is being expended in the optimisation of these ceramic composites systems, with particular emphasis being placed on the establishment of reliable and cost-effective fabrication procedures.[5–10] Mullite ($3Al_2O_3 \cdot 2SiO_2$) is one of the ideal oxide matrix materials for high temperature applications due to its good thermal shock resistance, low thermal expansion coefficient, high creep resistance and good chemical and thermal stability.[11,12] However, its low fracture toughness (1–3 M Pa $m^{-1/2}$) and high flaw sensitivity need to be increased for structural applications. One way to do this is by incorporating high-strength continuous ceramic fibres into the mullite matrix in order to activate debonding, delamination, crack deflection, fibre bridging and fibre pull-out mechanisms that will contribute to a non-linear stress-strain response and achievement of a high fracture energy.[1]

It has been shown that catastrophic failure of oxide fibre reinforced oxide matrix composites can be prevented using a very porous (up to 50 vol.%) ceramic matrix with no particularly optimised interface between fibre and matrix.[13] However, most theoretical models and experimental findings suggest that for obtaining maximised damage-tolerance and fracture toughness in fibre-reinforced brittle–matrix composites, tailored interphases between fibre and matrix providing optimised

* Corresponding author. Tel.: +44-121-4143537; fax: +44-121-4143441.
E-mail address: c.kaya@bham.ac.uk (C. Kaya).

0955-2219/02/$ - see front matter
PII: S0955-2219(01)00531-3

fibre/matrix bonding are required.[14–16] The essential properties of such an interphase are the ability to debond in the presence of transverse matrix microcracks and to transfer applied stress to the high strength/modulus fibres.[15] Micromechanical parameters such as interfacial shear stress (τ) and debonding energy (G_i), as well as long-term thermal stability of the interphase are the critical issues that have to be taken into consideration when a composite is fabricated. The critical characteristics of the interface can be summarised in terms of low interfacial fracture energy and moderate interfacial sliding resistance after debonding.[15,16] In an ideal fibre reinforced ceramic matrix composite the interphase should act as a reaction barrier between fibre and matrix, inhibit diffusion of atmospheric species to the fibres and remain intrinsically stable at high temperatures.[16] Many interphase materials including BN, carbon, ZrO_2, SnO_2, mica, mullite, $LaPO_4$ and porous refractory metals (Pt, Mo, etc.) have been introduced and applied to different matrices.[6,15–26] In particular, however, during the last decade oxide based interphase materials have been the focus point in the oxide–oxide ceramic composite field due to their long-term high temperature stability with respect to fibre, matrix and gaseous environments as well as their favourable shear and debonding characteristics and low fracture energies also at high temperatures.[6,24–26] Most studied compounds have the generic formula MXO_4 (monazite), where M is a rare earth ion in high oxygen coordination and X is the pentavalent metal ion which is tetrahedrally or octahedrally co-ordinated by oxygen. These complex oxides have a high probability of low cohesion with matrix or fibre due to polarisation of oxygen bonds by high valence cations. Phosphates and niobates are typical examples having the monazite structure. In the present study, $NdPO_4$ was chosen as a weak interface material because it is easy to synthesise from liquid precursors or by hydrolysis of colloidal mixtures of the constituent oxides, allowing for adequate control of the particle characteristics, such as size, shape and purity. $NdPO_4$ has a high melting point (1975 °C), is compatible with mullite and less susceptible to β-alumina formation in Al_2O_3-rich matrices than the La-phosphate.

In the present work, a mullite matrix containing nanosized pores was reinforced with $NdPO_4$-coated mullite fibres in order to optimise the non-brittle failure of the component by combining both the "porous-matrix" and "weak interface" concepts. Thermo-mechanical tests including high-temperature flexure strength and thermal cycling tests were carried out on the fabricated composites. The interrelationship between interphase structure and damage-tolerant behaviour in terms of fibre debonding, crack deflection and fibre pull-out were examined by electron microscopy observations of the interphase/fibre and interphase/matrix interfacial zones.

2. Experimental work

2.1. Matrix material preparation

A sinter-active and stoichiometric mullite ($3Al_2O_3 \cdot 2SiO_2$) powder containing 5 wt.% zirconia was synthesised using low-temperature hydrothermal processing, as reported in the literature.[27] The particles tend to be highly irregular in morphology with a wide particle size distribution, as determined by scanning electron microscopy (SEM) and particle size analysis, respectively. The as-produced mullite sol was vacuum filtered and the obtained powder was dried at 110 °C for 4 h followed by calcination at 850 °C for 3 h in order to produce coarser particles and so to reduce the amount of shrinkage that would occur during sintering. The calcined powders were ball-milled for 1 day using TZP balls and re-dispersed in water at a pH value of 3. The solids-loading of the suspension was kept constant at 20 wt.% with simultaneous ultrasonic agitation to enhance powder dispersion. The electrophoretic mobility and net surface charge of the mullite particles were measured as a function of dispersion pH using a surface-charge analyser (Delsa 440).

2.2. Preparation of interphase material ($NdPO_4$) and fibre coating

$NdPO_4$ powders suitable for the preparation of a stable suspension were synthesised by the direct reaction of neodymium oxide and phosphoric acid at room temperature, as described in the literature:[28]

$$Nd_2O_3 + 2H_3PO_4 = 2NdPO_4 + 3H_2O \quad (1)$$

The main advantage of this direct reaction between Nd_2O_3 and H_3PO_4 is that there is no by-product other than water. The resultant gel containing $NdPO_4$ and water was vacuum filtered and washed three times followed by drying at 110 °C for 3 h. The obtained dried powders were calcined at 1000 °C for 3 h to yield stoichiometric $NdPO_4$ monazite powders. Both SEM and transmission electron microsocopy (TEM) were used to investigate the $NdPO_4$ particle characteristics. In the final stage, $NdPO_4$ powders were dispersed in distilled water and a 15 wt.% stable suspension was prepared after ball-mixing for one day at a pH value of 3. This suspension was used to coat the composite reinforcing fibres.

Eight-harness satin woven mullite fibre mats (Nextel^{TM} 720, 3M, USA) were used as reinforcement material in the present composites. The fibre mats were pretreated by desizing at 500 °C for 1 h to remove the organic protection layer from the fibre surface. The fibre mats were then immersed in an ammonia based solution, consisting of an ammonium salt of polymethacrylic acid

(Versical KA21, pH: 9, Allied Colloids, UK) in order to create a strong negative surface charge on the fibre surface and to improve the wetting behaviour of the fibres. This process maximises the mutual electrostatic attraction between the fibre surface and the positively charged $NdPO_4$ particles (as determined by electrophoretic mobility measurements) in the coating suspension. During the coating process under vacuum, the fibre mats were immersed in the $NdPO_4$ suspension under sonication, causing the positively charged $NdPO_4$ particles to adhere to the negatively charged fibre surface. The immersed fibre mats were removed from the sol and dried in air for one day, and then finally fired at 600 °C for 0.5 h to strengthen the coating layer on the fibre surface.

2.3. Composite processing

An in-situ electrophoretic deposition (EPD) cell was used to infiltrate the $NdPO_4$-coated mullite fibre mats with matrix material. Detailed information about the development and application of this technique can be found elsewhere.[7,29,30] Coated fibre mats were attached to a stainless steel plate acting as deposition electrode, which was connected to the negative pole of a power supply. Another stainless steel plate served as the counter electrode. After the fibre preform was placed in the sol, the system was vacuum degassed to remove any entrapped air. The cell electrodes were connected to a 0–60 V d.c. power supply. A stable mullite aqueous suspension (pH = 3), as described in Section 2.1, was used. EPD was performed under constant voltage conditions (10 V d.c.) using a deposition time of 1 min. An electrode separation distance of 15 mm was used in all experiments and eight coated fibre mats were individually deposited. Under the applied electric field, the very fine mullite particles possessing a net positive surface charge, as determined from the electrophoretic mobility data, migrated towards the negative electrode. The particles infiltrated the fibre tows and deposited until a sufficient matrix thickness, which enveloped the fibre tows, was achieved.

Eight electrophoretically deposited fibre mats were then placed in a high-load pressure filtration (PF) assembly to form the green body (in the form of flat cylinders of 70 mm diameter). The PF procedure has been described in detail elsewhere.[29] The EPD-infiltrated and pressure filtrated green body specimens were subsequently dried under humidity-controlled atmosphere for 1 day and left in normal air for another day before being pressureless sintered at 1200 °C for 3 h in air.

2.4. Flexural tests at room and elevated temperatures

Flexural test bars were cut from the sintered discs using an Accutom 5 high-speed, precision diamond saw, and then both surfaces were ground to be parallel using a 40-μm diamond, resin bonded disc. All sharp edges were bevelled using 6-μm diamond paste on a soft cloth in order to minimise possible flaw sources. The tensile surfaces were then polished to a 0.25 μm finish using diamond paste. Room and high-temperature four-point flexure strength tests were performed on an Instron Testing machine fitted with a furnace which has tungsten mesh elements enabling tests to be carried out at temperatures up to 1500 °C. The pushrods and fixtures are all made from a tungsten-zirconium-molybdenum alloy. Specimens to be tested at elevated temperatures were held at the test temperature for at least an hour prior to testing to allow the system to equilibrate and to ensure that the specimen was at this temperature. Flexural tests were carried out at a constant displacement rate of 0.5 mm/min using a test fixture having outer and inner spans of 40 and 20 mm, respectively. The span (S) to specimen thickness (h) ratio was chosen to be sufficient large ($S/h > 10$) to avoid large shear delamination forces.

2.5. Thermal cycling tests

Thermal cycling tests on samples of prismatic shape, suitable for flexural strength tests, were conducted using a computer-controlled rig. A cycling program was applied to induce heating and cooling between 25 and 1150 °C and an isothermal hold time of 15 min. These tests were carried out in laboratory air. The applied cycles resulted in a heating/cooling rate of about 900 °C per min at the initial stages, which gradually reduced to approximately 500 °C/min as the temperature approached the limits of the cycle. Temperature was measured by two different thermocouples attached to the samples.

After thermal cycling the samples were visually inspected for the presence of macroscopic surface damage, such as delamination, chipping or fibre protrusion. Selected thermal cycled specimens were tested at room temperature in flexure strength configuration, as described above.

2.6. Microstructural characterisation

Mullite powder and sintered samples were analysed using X-ray diffraction (CuK_α radiation and nickel filter to remove the Cu K_β peak, Philips X'Pert, Germany), operated at 40 keV and 30 mA. The diffractometer scanned from 5 to 80° with a scan step of 0.02° 2θ and a count time of 2 s per step. Microstructural examinations on sintered monolithic mullite and fibre-reinforced composites were also carried out using a high-resolution Field Emission Gun SEM (FEG SEM FX-4000, Jeol Ltd. Japan). The interfacial microstructure between the $NdPO_4$ interphase and the mullite matrix and between the $NdPO_4$ interphase and the mullite fibres was examined using a Jeol 4000 FX TEM operating at 400 keV, and equipped with an energy dispersive X-Ray analysis

(EDX) unit. The surfaces of selected thermally cycled samples were also observed by SEM.

3. Results and discussion

3.1. Materials characterisation

The particle size distribution results and a SEM micrograph of the hydrothermally synthesised mullite plus 5 wt.% zirconia powder used in this work are shown in Fig. 1. The cumulative statistics shown in Fig. 1(a) for as-produced powder is given as D_{25}, D_{50}, D_{75} and D_{90} values, which indicate the particle sizes below which are 25, 50, 75 and 90% of the total volume of particles analysed, respectively. Particle size distribution is a very critical issue in green body formation using EPD or pressure filtration. A mixture of coarse, medium and very fine particles, where sufficient fine particles are present to fill in the interstices, results in a green body compact of high green density. As shown in Fig. 1b, there are some very fine particles (as fine as 55 nm) within the synthesised powders as well as very coarse ones (7.1 μm). However, the mean particle size is in the range of 2–3 μm. Fig. 1b also shows the presence of very fine (20–30 nm) zirconia precipitates located within the mullite particles and these very fine particles are expected to enhance the sintering rates of monophasic mullite powders via controlling grain growth. Overall, the very fine particles (<100 nm) are considered to be ideal for

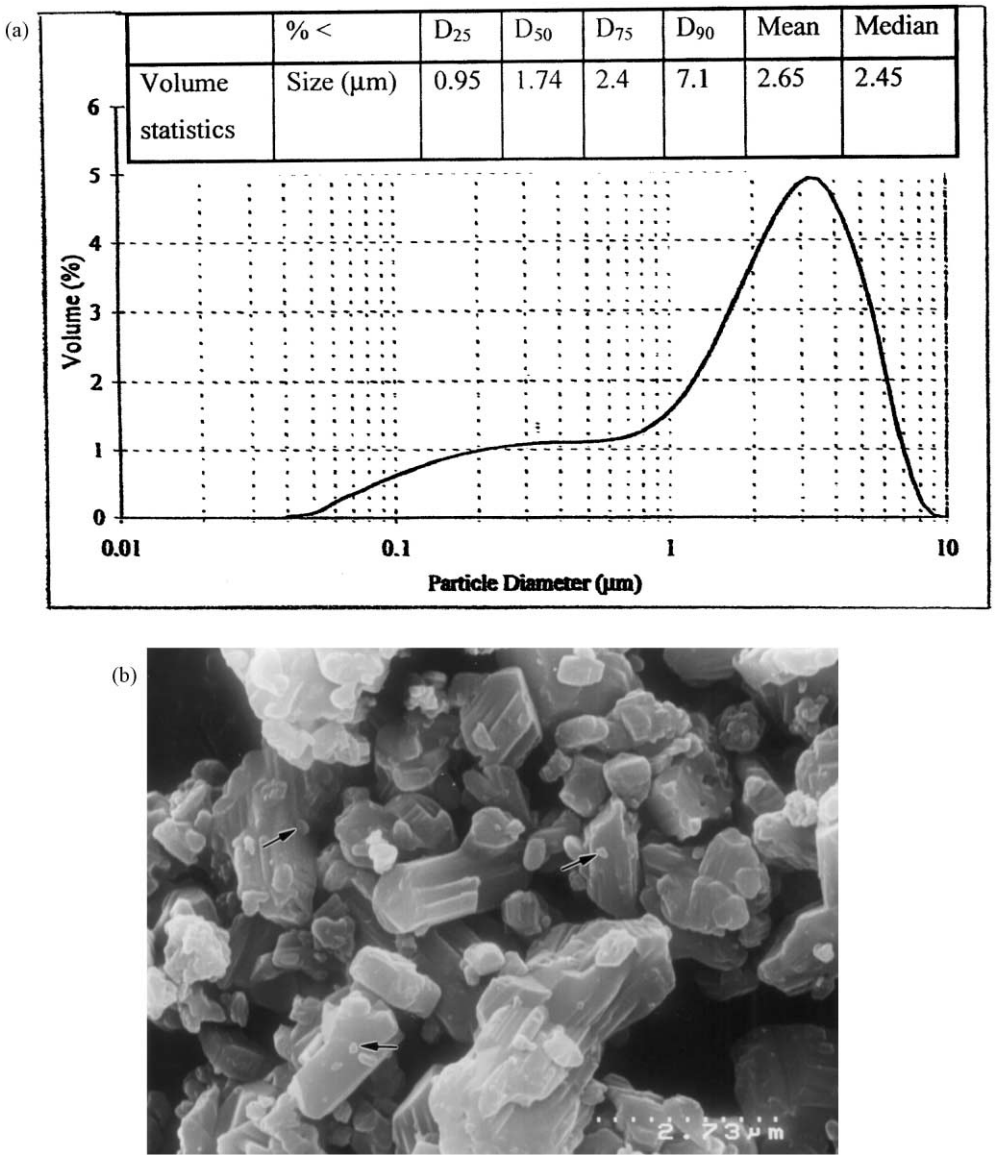

Fig. 1. (a) Particle size analysis and (b) SEM micrograph of the hydrothermally synthesised mullite plus 5 wt.% zirconia powder showing the presence of very fine (20–30 nm) zirconia precipitates (as arrowed) within the mullite particles.

electrophoretic deposition as the particle mobility and deposition behaviour during EPD will be enhanced.[7,29,30]

The electrophoretic mobility data in terms of particle net surface charge and mean particle size for the mullite powder and the $NdPO_4$ aqueous sol suspensions at a constant pH value of 3 are shown in Table 1. From these data, it is evident that both particles are positively-charged at a pH value of 3, therefore if any particles are required to be attracted to the target material (for example to the electrodes during EPD or to the fibre surface during dip coating), the surface charge of such substrates has to be controlled to be opposite of the deposited material. The net surface charge around a particle is a very critical parameter in EPD and dip-coating processes in order to obtain maximum deposition and coating efficiency using the "mutual electrostatic attraction" concept.

3.2. Characterisation of the interphase material ($NdPO_4$)

The key issues in the dip coating process are the extent of wetting of the fibres by the sol and the electrostatic attraction between the fibre surface and coating particles.[16,18,31] However, the characteristics of the coating particles dispersed in a suspension in terms of their shape, size and surface charge have to be taken into consideration as they affect the coating behaviour significantly. The TEM micrograph shown in Fig. 2a indicates that the synthesised $NdPO_4$ particles are of near spherical shape and the particle size is in the range of 10–70 nm, with a mean particle size of 30 nm (as determined by particle size analysis). In order to determine the microstructure of the interphase after sintering, a sample prepared from the coating suspension containing $NdPO_4$ powders was prepared using simple die pressing and then sintered at 1200 °C for 3 h (the same sintering temperature used for the final composite). The SEM micrograph of the sintered microstructure obtained is shown in Fig. 2b. It is seen that the $NdPO_4$ body has a plate-like grain microstructure with the presence of no intra- or inter-granular porosity indicating the dense nature of the material. This microstructure provides, when used as an interphase in a composite, a weak bonding with both matrix and fibre (i.e. the required weak interfaces),[1] leading to the desired fibre debonding, crack deflection and fibre pull-out mechanisms.

Fig. 3a shows a SEM microstructure of a fibre, which has been dip-coated with $NdPO_4$ without fibre pre-treatment, indicating the poor quality of the coating as a result of the absence of electrostatic attraction between the fibre and coating particles. However, when the fibre surface is conditioned with a high pH solution prior to coating in order to create a strong negative surface charge, successful results of mullite fibres coated with $NdPO_4$ particles are achievable, as shown in Fig. 3b after thermal treatment at 600 °C for 0.5 h. The image indicates that the coating is homogeneous over the fibre surface and its thickness is approximately 2.5 μm. One of the significant disadvantages associated with dip coating is the excess deposition of the coating particles in the inter-fibre regions, generally resulting from the presence of large flocculated chains within the coating sol. As shown in Fig. 3c, $NdPO_4$ particles did not fill the regions between individual fibres within the woven mat structure and during dip coating under the application of vacuum, the capillary pressure difference across the

Table 1
Surface charge properties and mean particle size of the hydrothermally synthesised mullite plus 5 wt.% zirconia and $NdPO_4$ coating powders dispersed in water at a pH value of 3

	Electrophoretic mobility (10^{-8} m^2 $V.s^{-1}$)	Mean particle size
Mullite + 5 wt.% ZrO_2, pH: 3	+1.97	2.65 μm
$NdPO_4$, pH: 3	+2.78	30 nm

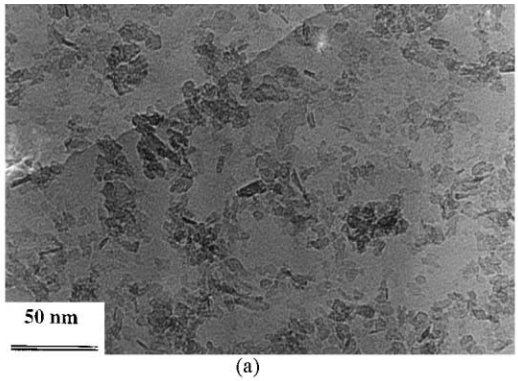

(a)

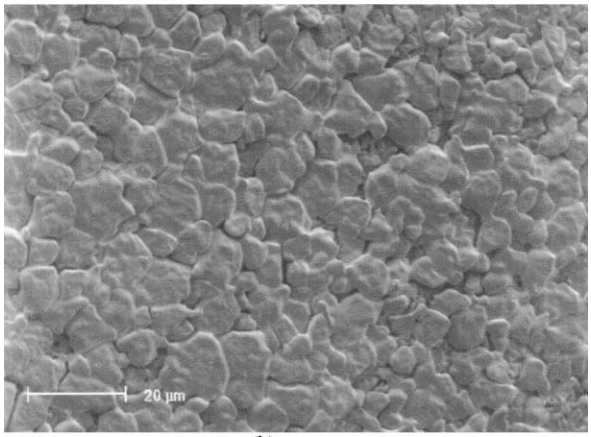

(b)

Fig. 2. (a) TEM micrograph of synthesised $NdPO_4$ particles indicating their near spherical shape and (b) SEM micrograph showing the dense sintered microstructure of $NdPO_4$ material after sintering at 1200 °C for 3 h.

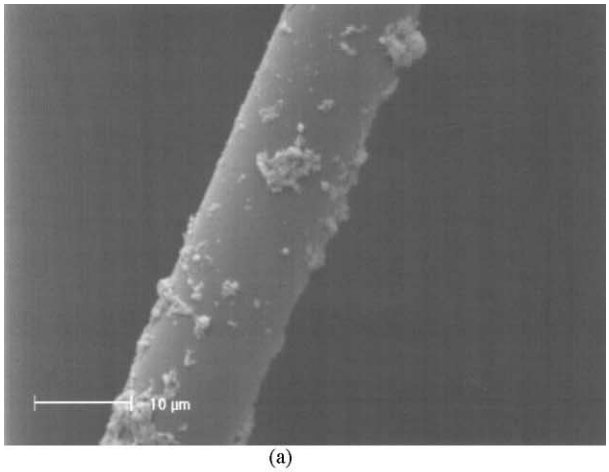

(a)

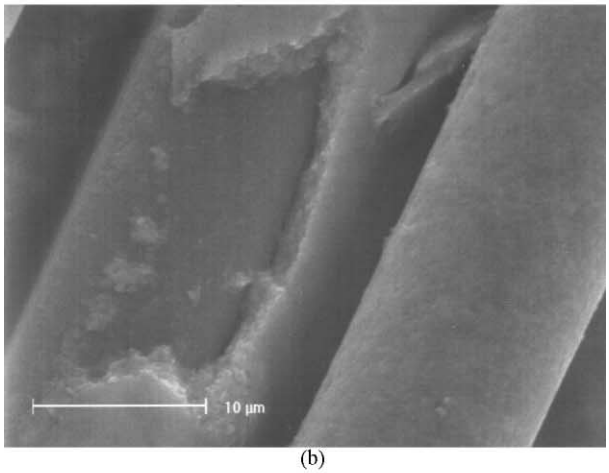

(b)

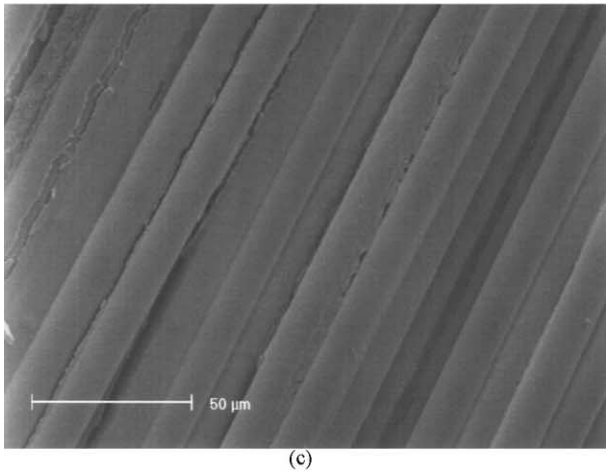

(c)

Fig. 3. SEM micrographs of mullite fibres after dip-coating in $NdPO_4$ suspension, showing: (a) poor coating quality if the fibre surface is not pre-treated with a high pH sol prior to coating, (b) homogeneous $NdPO_4$ coating around the mullite fibre surface obtained by dip coating when the fibre surface is pre-treated and (c) successfully coated mullite fibre mat with very fine $NdPO_4$ particles. Note that coated fibres shown here have been fired at 600 °C and the average coating thickness is about 2 μm.

curved fibre surfaces was increased resulting in enhanced coating only on the fibre surface.[18,32] Under these conditions, $NdPO_4$ particles were deposited onto the fibres by improved electrostatic attraction leading to the formation of the coating layer whilst the fibre mat was immersed in the coating suspension, as shown in Fig. 3c. The effectiveness of fibre surface treatment is thus demonstrated in Fig. 3b and c, indicating the homogeneous and full coverage of the fibre surface and woven fibre mat layer by the monazite particles due to the strong mutual electrostatic attraction.

The results presented in Figs. 2 and 3 provide additional information about the relationship between the nature of monazite interface and the coating quality. In a previous work, it has been shown that the needle-like morphology and coarse particle size (400 nm) of $NdPO_4$ inhibit the infiltration process and result in poor coating of mullite fibres.[14] It appears from the present results that the very fine (30 nm) and more equiaxed morphology of coating particles enhances the homogeneous coating, proving that dip-coating is an appropriate method for coating woven fibre fabric layers rather than individual fibres. Fibre surface pre-treatment with a wetting agent prior to dip-coating is also shown to be a critical step in order to obtain a high-quality coating layer.

3.3. Electrophoretic deposition and pressure filtration

The SEM micrographs in Fig. 4 show the microstructures of the EPD-infiltrated and pressure filtrated mullite fibre-reinforced mullite composites with a $NdPO_4$ interphase. $NdPO_4$-coated mullite woven fibre mats were nearly fully infiltrated by the mullite powders during EPD and pressure filtration as the green microstructure in Fig. 4a demonstrates. As can be seen the intra-tow regions of the woven fibre mat are well infiltrated. The sintered microstructure is shown in Fig. 4b indicating the absence of any drying or sintering cracks within the composite after sintering at 1200 °C for 3 h, resulting in a relatively high density of 86% of theoretical density (TD). Matrix phase composition was found to be stoichiometric 3:2 mullite plus zirconia (monoclinic form) using XRD, as shown in Fig. 5a. No residual cristobalite was found under the detection limit of XRD. The sintered microstructure of mullite plus 5 wt.% zirconia matrix is shown in Fig. 5b. The image was taken from a sample fractured at room temperature indicating the presence of homogeneously distributed very fine (50–350 nm in diameter) spherical pores within the mullite grains and also on the grain boundaries. This microstructural feature is due to the hydrothermal processing of the mullite powders and it is considered to be a convenient feature to obtain both good thermal shock resistance and high temperature damage-tolerant behaviour.

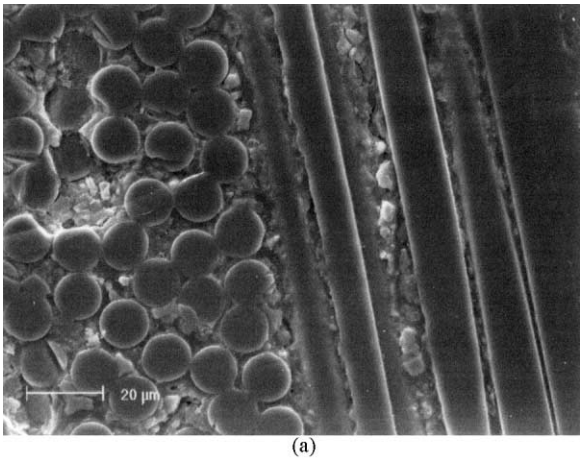

(a)

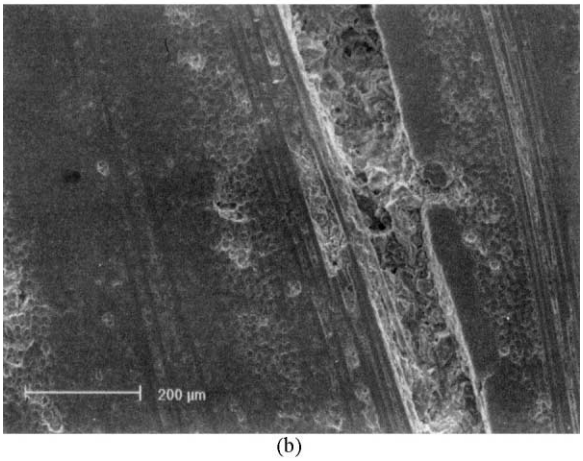

(b)

Fig. 4. SEM micrographs of mullite fibre-reinforced mullite matrix composites with $NdPO_4$ interface fabricated by electrophoretic deposition and pressure filtration indicating; (a) green microstructure after drying and (b) sintered microstructure after pressureless sintering at 1200 °C for 3 h. The sintered composite contains approximately 35 vol.% fibre and has a relative density of 86.4%TD.

3.4. Thermomechanical performance

The flexure strength values as a function of test temperature are given in Table 2. As can be seen from the table, the maximum strength value (235 MPa) is obtained at room temperature, but strength data are not affected significantly by the test temperature up to 1300 °C, which provides a strength value of 230 MPa.

Table 2
Four-point flexural strength of mullite fibre-reinforced mullite matrix composites with $NdPO_4$ interphase as a function of test temperature

Test temperature (°C)	Four-point flexural strength (MPa)
RT	235±32
1000	234±17
1200	233±33
1300	230±41

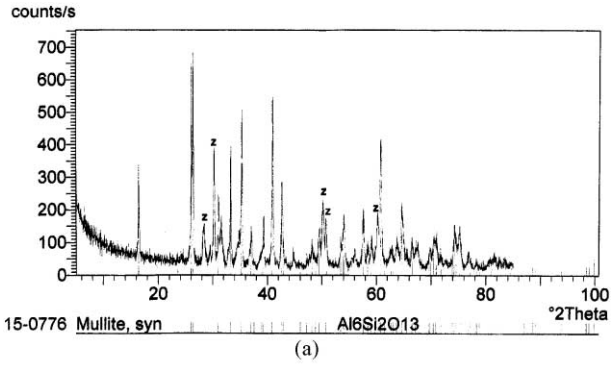

(a)

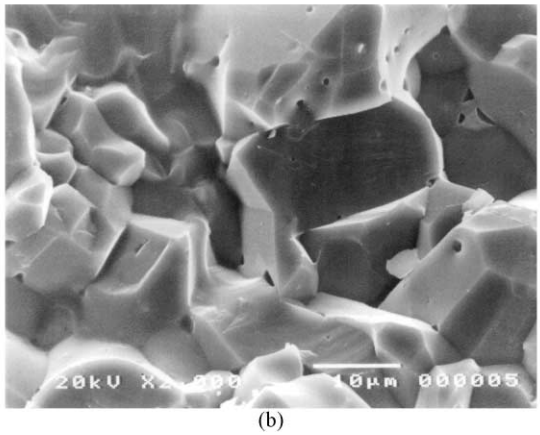

(b)

Fig. 5. (a) X-ray (CuK_α) diffraction pattern for the sintered mullite matrix produced from hydrothermally synthesised mullite/5 wt.% zirconia powder showing also the standard pattern for the 3:2 mullite (JCPDS card no: 15–0776). The peaks labelled Z are for monocilinic zirconia and the other peaks represent orthorhombic mullite. (b) SEM micrograph of the mullite matrix showing the presence of very fine pores (as arrowed) in both inter- or trans-granular locations.

Fig. 6a shows stress-deflection curves of the composites at room temperature and at 1300 °C, as obtained in the four-point flexure strength test. The shape of the curves suggests that the composite exhibits "pseudo-plastic" deformation and damage tolerant behaviour, which should result from the presence of the optimised interphase material ($NdPO_4$).

The SEM micrographs of fracture surfaces tested at room and elevated (1300 °C) temperatures are given in Fig. 6b and c, respectively, both indicating the presence of damage-tolerant behaviour with long fibre pull-out lengths. Although mullite fibres of the type used here may suffer from significant strength loss at temperatures higher than 1200 °C,[33] the composites produced in this work do not show dramatic strength decrease at 1300 °C. This behaviour may result from two factors: the nature of the interphase and the mullite matrix microstructure. As shown in Figs. 2b and 3b and c, the $NdPO_4$ interphase material is very dense but there is no reaction with fibre or matrix, therefore there is no reaction product in the fibre/matrix zone. Secondly, as shown in Fig. 5b, the mullite matrix has some residual porosity particularly at the inter-fibre tow regions, thus

crack deflection (and/or crack arrest) may take place within the matrix as well as at the interphase/fibre and interphase/matrix interfaces both promoting the damage-tolerant behaviour. The occurrence of crack deflection and the presence of extensive fibre pull-out at room temperature and at 1300 °C are evident from the stress-displacement curves shown in Fig. 6a and from the SEM micrographs shown in Fig. 6b and c. Linear elastic deformation is recorded until the first matrix crack is formed at the maximum stress and then the dominant mechanisms are fibre pull-out and debonding until the composite fails in a non-catastrophic manner.

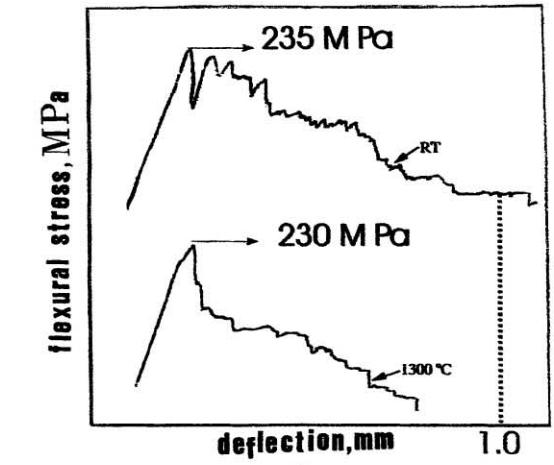

(a)

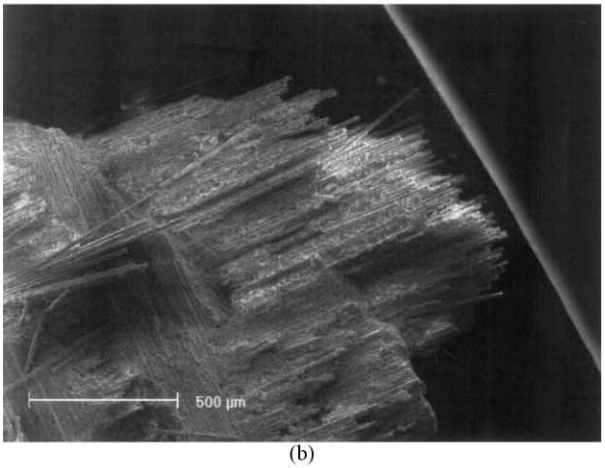

(b)

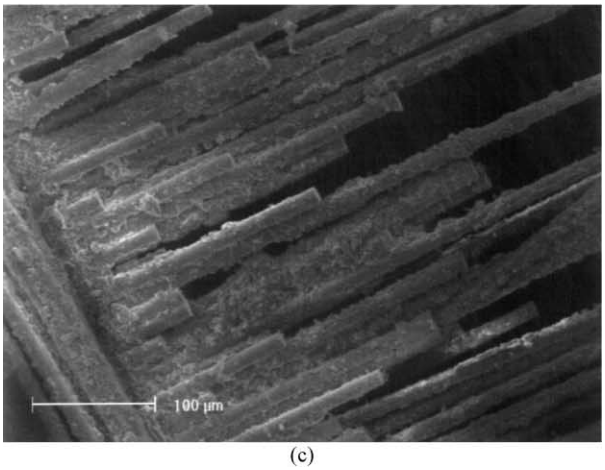

(c)

Fig. 6. (a) Stress-deflection curves for mullite fibre-reinforced mullite matrix composites with $NdPO_4$ interface obtained in flexure strength test at room temperature and at 1300 °C, (b) SEM micrograph of the fracture surface of the composite tested at room temperature and (c) SEM micrograph of the fracture surface of the composite tested at 1300 °C.

TEM observations were carried out along with EDX analysis on a sample tested at 1300 °C to investigate in detail the microstructure of the zones between $NdPO_4$ and fibre and between $NdPO_4$ and matrix, as shown in Fig. 7. This was also carried out in order to identify any possible reaction products caused by the reactions at the relevant interfaces. TEM observation coupled with EDX analysis of the interfacial regions (interphase/matrix and interphase/fibre) revealed that there was no reaction zone or new product formation during composite sintering or high temperature testing, as shown in Fig. 7a and b. It is also clear from both pictures that the interphase is very dense but bonding between interphase and matrix and between interphase and fibre is sufficiently weak, leading to the occurrence of fibre debonding, crack deflection and fibre pull out during composite failure.

The acceptable thermomechanical behaviour of the composite was also confirmed by the thermal cycling tests conducted from a high temperature of 1150 °C, as the results in Table 3 show. After up to 300 cycles, the samples retained a high flexural strength (> 85% of the strength of the as-fabricated material). Moreover the fracture behaviour of the thermally cycled samples was "quasi-ductile" and similar to that of the as-fabricated specimens. A SEM micrograph showing the surface of a thermally cycled sample is shown in Fig. 8. No formation of microcracks or evidence of other surface microstructural damage can be observed, indicating that the conditions investigated (thermal cycling between room temperature and 1150 °C in air) are not severe enough to cause damage in these composites. Whether or not the presence of a fine dispersion of closed pores in the matrix (Fig. 5b) is beneficial for the enhancing the thermal cycling resistance of the composites remains to be investigated. Experiments are planned using more

Table 3
Variation of flexural strength of mullite fibre-reinforced mullite matrix composites with $NdPO_4$ interphase after thermal cycling between room temperature and 1150 °C for different number of cycles

Number of cycles	Four-point flexural strength (MPa)
0	235
95	231
220	207
300	201

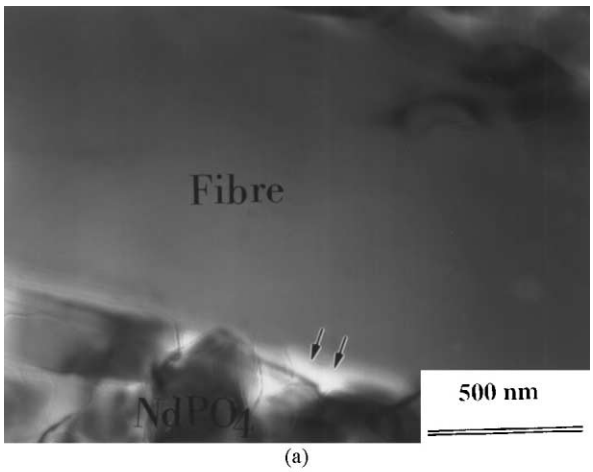

(a)

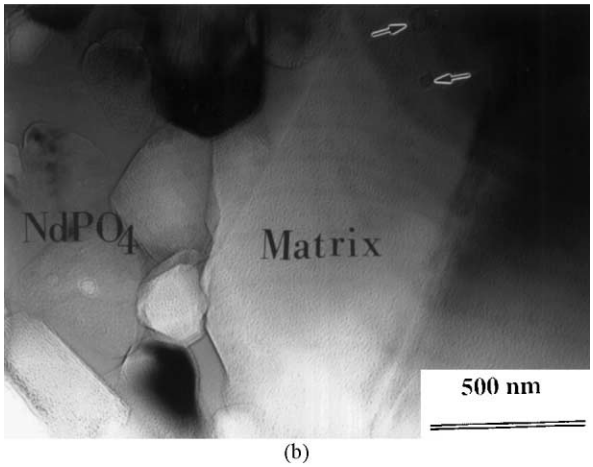

(b)

Fig. 7. Bright-field TEM images of the interfacial zones between (a) $NdPO_4$ interphase–mullite fibre and (b) $NdPO_4$ interphase–mullite matrix, both showing the absence of any reaction products or zone in these regions.

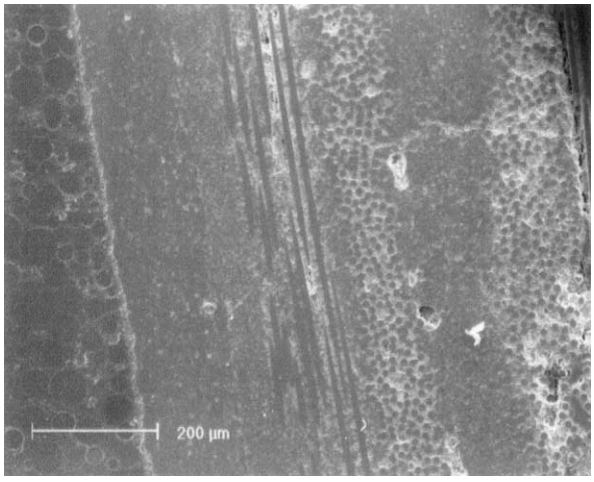

Fig. 8. SEM micrograph of the surface of a thermally cycled sample, showing no evidence of microcracking or of other form of superficial damage.

severe thermal cycling conditions, e.g. by using forced air cooling and higher cycle frequency.

4. Conclusions

A damage-tolerant mullite fibre (Nextel™ 720)-reinforced mullite matrix composite with a weak $NdPO_4$ interphase was successfully produced using electrophoretic deposition and pressure filtration techniques followed by pressureless sintering. The composite produced is capable of retaining room temperature flexural strength and damage-tolerance at elevated temperatures (1300 °C), as a result of the dense, chemically and thermally stable $NdPO_4$ interphase and the weak bonding between this interphase and both the matrix and fibres. Thermal cycling from 1150 °C to room temperature did not result in appreciable damage of the composite, and the samples retained a high flexural strength and "composite" behaviour after thermal cycling for up to 300 cycles. It is concluded that the dense $NdPO_4$ interphase improves damage-tolerant behaviour at room and high temperatures if: (1) the bonding at the interfaces interphase-fibre and interphase-matrix is weak enough, which leads to extensive fibre debonding, crack deflection and fibre pull-out, and (2) the mullite matrix contains porosity with homogeneously distributed fine pores.

Acknowledgements

Professors M.H. Loretto and P. Bowen are acknowledged for the provision of laboratory facilities at the IRC and School of Metallurgy and Materials, at the University of Birmingham, respectively. Partial financial support by the European Commission under the contract numbers BRITE-EURAM CT 97–0609 and CT 95–0110 is also acknowledged. ARB acknowledges support of the Nuffield Foundation (London).

References

1. Evans, A. G. and Marshall, D. B., High toughness ceramics and ceramic composites. *Progress in Materials Science*, 1989, **33**, 85–90.
2. Warren, R. and Deng, S., Continuous fibre reinforced ceramic composites for very high temperatures. *Silicates Industriels*, 1996, **5**(6), 99–107.
3. Chawla, K. K., The high-temperature application of ceramic matrix composites. *JOM- J. Min. Met. Mater.*, 1995, **47**, 19–21.
4. Porter, J. R., Reinforcements for ceramic–matrix composites for elevated temperature applications. *Mater. Sci. Eng.*, 1993, **A166**, 179–184.
5. Holmquist, M., Lundberg, R., Sudre, O., Razzell, A. G., Molliex, L., Benoit, J. and Adlerborn, J., Alumina/alumina composite with a porous zirconia interphase, processing, properties and component testing. *J. Eur. Ceram. Soc.*, 2000, **20**, 599–606.
6. Chawla, K. K., Coffin, C. and Xu, Z. R., Interface engineering in oxide fibre/oxide matrix composites. *Int. Mater. Rev.*, 2000, **45**, 165–189.

7. Boccaccini, A. R., Kaya, C. and Chawla, K. K., Use of electrophoretic deposition in the processing of fibre reinforced ceramic and glass matrix composites. A review, *Composite Part A*, 2000, **32**, 997–1006.
8. Kanka, B. and Schneider, H., Aluminosilicate fiber/mullite matrix composites with favorable high-temperature properties. *J. Eur. Ceram. Soc.*, 2000, **20**, 619–623.
9. Kramb, V. A., John, R. and Zawada, L. P., Notched fracture behaviour of an oxide/oxide ceramic matrix composite. *J. Am. Ceram. Soc.*, 1999, **82**, 3087–3096.
10. Peters, P. W. M., Daniels, B., Clements, F. and Vogel, W. D., Mechanical characterisation of mullite-based ceramic matrix composites at test temperatures up to 1200 °C. *J. Eur. Ceram. Soc.*, 2000, **20**, 531–535.
11. Aksay, I. A. and Pask, J. A., Stable and metastable equilibria in the system SiO_2–Al_2O_3. *J. Am . Ceram. Soc.*, 1975, **58**, 507–512.
12. Dokko, P. C., Pask, J. A. and Mazdiyashi, K. S., High-temperature mechanical properties of mullite under compression. *J. Am. Ceram. Soc.*, 1977, **60**, 150–155.
13. Tu, W. C., Lange, F. F. and Evans, A. G., Concept for a damage-tolerant ceramic composite with "strong" interfaces. *J. Am. Ceram. Soc.*, 1996, **79**, 417–424.
14. Lewis, M. H., Tye, A., Butler, E. and Al-Dawery, I., Development of interfaces in oxide matrix composites. *Key Engineering Materials*, 1999, **164**(165), 351–356.
15. Kuo, D.-H., Kriven, W. M. and Mackin, T. J., Control of interfacial properties through fibre coatings: monazite coatings in oxide–oxide composites. *J. Am. Ceram. Soc.*, 1997, **80**, 2987–2996.
16. Lewis, M. H., Tye, A., Butler, E. G. and Doleman, P. A., Oxide CMCs: interphase synthesis and novel fibre development. *J. Eur. Ceram. Soc.*, 2000, **20**, 639–644.
17. Schmuecker, M., Schneider, H., Chawla, K. K., Xu, Z. R. and Ha, J.-S., Thermal degradation of fibre coatings in mullite-fibre-reinforced mullite composites. *J. Am. Ceram. Soc.*, 1997, **80**, 2136–2140.
18. Gu, X., Trusty, P. A., Butler, E. G. and Ponton, C. B., Deposition of zirconia sols on woven fibre preforms using a dip-coating technique. *J. Eur. Ceram. Soc.*, 2000, **20**, 675–684.
19. Ha, J.-S., Chawla, K. K. and Engdahl, E. E., Effect of processing and fiber coating on fibre matrix interaction in mullite fibre–mullite matrix composites. *Mat. Sci and Eng.*, 1993, **A161**, 303–308.
20. Davies, J. B., Löfvander, J. P. A., Evans, A. G., Bischoff, E. and Emiliani, M. L., Fibre coating concepts for brittle-matrix composites. *J. Am. Ceram. Soc.*, 1993, **76**, 1249–1257.
21. Kaya, C., Boccaccini, A. R. and Chawla, K. K., Electrophoretic deposition forming of nickel-coated-carbon-fibre-reinforced borosilicate–glass–matrix composites. *J. Am. Ceram. Soc.*, 2000, **83**, 1885–1888.
22. Wendorff, J., Janssen, R. and Claussen, N., Platinum as a weak interphase for fiber-reinforced oxide-matrix composites. *J. Am. Ceram. Soc.*, 1998, **81**, 2738–2740.
23. Morgan, P. E. D. and Marshall, D. B., Functional interfaces for oxide/oxide composites. *Mater. Sci. Eng. A*, 1993, **A162**, 15–25.
24. Morgan, P. E. D. and Marshall, D. B., Ceramic composites of monazite and alumina. *J. Am. Ceram. Soc.*, 1995, **78**, 1553–1563.
25. Kaya, C, Butler, E. G., Boccaccini, A. R. and Lewis, M. H., Processing and characterisation of mullite (Nextel™ 720) fibre-reinforced mullite matrix composites from hydrothermally processed mullite precursors. In *High Temperature Ceramic Matrix Composites (HT-CMC 4)*, ed. W. Krenkel, R. Naslain and H. Schneider. Wiley-VCH, Weinheim, Germany, 2001, pp. 639–644.
26. Chawla, K. K., Liu, H., Janczak-Rusch, J. and Sambasivan, S., Microstructure and properties of monazite ($LaPO_4$) coated saphikon fiber/alumina matrix composites. *J. Eur. Ceram. Soc.*, 2000, **20**, 551–559.
27. Kaya, C., Kaya, F. and Trusty, P. A., Hydrothermal synthesis of 3:2 mullite ($3Al_2O_3{\cdot}2SiO_2$) + 5 wt.% ZrO_2 powders for use as a high temperature porous matrix. *J. Mater. Sci* (in press).
28. Chen, P. and Mah, T., Synthesis and characterisation of lanthanum phosphate sol for fibre coating. *J. Mater. Sci.*, 1997, **32**, 3863–3867.
29. Kaya, C., Processing and Properties Of Alumina Fibre-reinforced Mullite Ceramic Matrix Composites, PhD thesis, The University of Birmingham, UK, June 1999.
30. Kaya, C., Kaya, F., Boccaccini, A. R. and Chawla, K. K., Fabrication and characterisation of Ni-coated carbon fibre-reinforced alumina ceramic matrix composites using electrophoretic deposition. *Acta Mater.*, 2001, **49**, 1189–1197.
31. Hay, R. S., Sol-gel coating of fibre tows. *Ceram. Eng. Sci. Proc*, 1991, **12**, 1064–1074.
32. Adamson, A. W., *Physical Chemistry of Surfaces,* 4th edn. Wiley, New York, 1982.
33. Petry, M. D. and Mah, T., Effect of thermal exposures on the strengths of nextel™ 550 and 720 filaments. *J. Am. Ceram. Soc.*, 1999, **82**, 2801–2807.